DFT Investigation of the $\eta(6)$ $\eta(6)$-Inter-ring Haptotropic Rearrangement of the Group 8 Metals Complexes [(graphene)MCp](+) (M = Fe, Ru, Os)

Igor P Gloriozov, Piotr I Dem'yanov, Nikolay S Zhulyaev, Mikhail S Nechaev, Yuri F Oprunenko, Franck Gam, Jean-Yves Saillard, Aleksey E Kuznetsov

DFT Investigation of the $\eta^6 \rightleftharpoons \eta^6$-Inter-Ring Haptotropic Rearrangement of the Group 8 Metals Complexes [(graphene)MCp]$^+$ (M=Fe, Ru, Os)

Igor P. Gloriozov,[a] Piotr I. Dem'yanov,[a] Nikolay S. Zhulyaev, [a] Mikhail S. Nechaev,[a, b] Yuri F. Oprunenko,[a] Franck Gam,[c] Jean-Yves Saillard,[c*] and Aleksey E. Kuznetsov[d]*

[a]Department of Chemistry, M.V. Lomonosov Moscow State University, Leninskie Gory 1, Building 3, 119991 Moscow, Russia

[b]A. V. Topchiev Institute of Petrochemical Synthesis, Russian Academy of Sciences, Leninsky Prospect 29, 119991 Moscow, Russia

[c]Univ Rennes, CNRS, ISCR-UMR 6226, F-35000 Rennes, France

[d]Department of Chemistry, Universidad Técnica Federico Santa Maria 6400, Vitacura 7660251, Santiago, Chile

ABSTRACT

Transition metal complexes are well known for their catalytic applications in the design of novel derivatives, technological precursors, or advantageous materials for various areas of science and industry. Catalytic properties of metalcyclopentadienyl complexes $(MCp)^+$ complexes of polyaromatic hydrogenated hydrocarbons (PAHs) are mainly associated with their structural peculiarities along with their capacity for inter-ring haptotropic rearrangements (IRHRs) that occur usually via intra-molecular mechanisms. IRHRs consist of the shifting of the ML_n organometallic group (OMG) along the PAH plane. Large PAHs such as graphene and nanotubes possess intrinsic anticancer activity, and numerous arene complexes of Ru and Os have been proven to have anticancer properties as well. We suppose that coordinating Ru or Os to very large PAHs could synergistically increase the anticancer activity. Therefore, the metalcyclopentadienyl complexes $(MCp)^+$ (M = Fe, Ru, Os) bound to the large PAH $C_{96}H_{24}$ used as a model for pristine graphene have been studied using density functional theory (DFT) approach to reveal their structural features and dynamic behavior. The inter-ring haptotropic rearrangements for these complexes were shown to occur via two transition states and one intermediate. The energy barriers of the $\eta^6 \rightleftharpoons \eta^6$ IRHRs of the $(MCp)^+$ unit were found to be 30, 27, and 29 kcal/mol for M = Fe, Ru, Os, respectively. These values are significantly lower than the values found previously for smaller PAHs. Both polar and nonpolar solvents were found not to affect significantly the energy barrier height.

KEYWORDS: Cyclopentadienyliron(II), cyclopentadienylruthenium(II), cyclopentadienyl-osmium(II), graphene-like complexes, inter-ring haptotropic rearrangement (IRHR), DFT calculations

Corresponding authors e-mails:

Dr. Jean-Yves Saillard: jean-yves.saillard@univ-rennes1.fr

Dr. Aleksey E. Kuznetsov: aleksey.kuznetsov@usm.cl

Transition metal complexes are well known for their catalytic applications in the design of novel derivatives and technological precursors (e.g., for polymers) or advantageous materials for various areas of science and industry (sensors, catalysts, etc.).[1-8] Catalytic properties of $(MCp)^+$ complexes of polyaromatic hydrogenated hydrocarbons are mainly associated with their structural peculiarities along with their capacity for inter-ring haptotropic rearrangements (IRHRs) that occur usually via intra-molecular mechanisms.[9-10] IRHRs consist of the shifting of the ML_n organometallic group (OMG) along the PAH plane, from one six-membered ring to another. In the course of such rearrangements, the metal acquires unsaturation and therefore can easily seize additional substrates and/or reagents into its coordination sphere. In general, the $\eta^n \rightleftharpoons \eta^n$-IRHRs of the ML_n OMGs have been observed for many transition metal complexes with PAHs (Scheme 1, *e.g.*, n = 6, M = Cr,[11-13] Ru;[14-18] n = 4, M = Ir;[19] n = 2, M = Ni[20]), but have been principally investigated for $\eta^6 \rightleftharpoons \eta^6$-IRHR of chromium tricarbonyl complexes.[11-13] In the course of such IRHRs, the 12-electron ML_n OMG migrates along the periphery of a polyaromatic plane, as shown by Albright *et al.*[12] These migrations could be induced not only thermally[11-13] but also chemically,[13] photochemically[14-17] or electrochemically.[18]

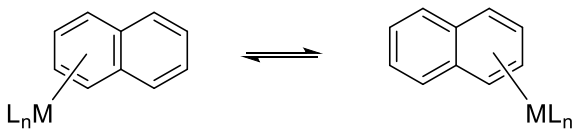

Scheme 1. Some examples of $\eta^n \rightleftharpoons \eta^n$-IRHRs in OMG complexes of naphthalene or substituted naphthalene (n = 6: ML_n = $Cr(CO)_3$,[11-13] $(RuCp)^+$;[14-18] n = 4: ML_n = $Ir(PR_3)_2$;[19] n = 2, ML_n = $Ni(PR_3)_2$[20]).

In spite of the fact that the Group 8 $(MCp)^+$ complexes of PAHs and their dynamic behavior are quite important in such applications as catalysis[14,21-28] or antitumor agents,[29-36] only a very small number of $\eta^6 \rightleftharpoons \eta^6$-IRHRs of these OMGs have been observed so far. Moreover, they are restricted to Ru[18,37] and so far no data concerning Fe or Os have been obtained.[38,39] For example, such IRHRs were observed for ruthenium complexes of non-planar PAHs, namely the concave acecorannulene[40] and the propeller-like rubrene[41] (Scheme 2).

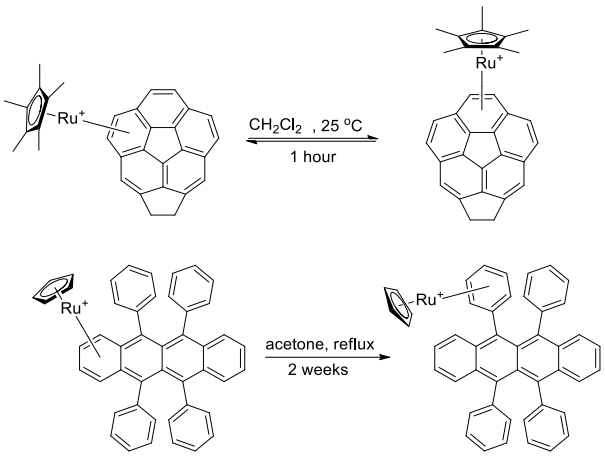

Scheme 2. IRHRs for $(RuCp)^+$ and $(RuCp^*)^+$ complexes of non-planar PAHs.

The reaction kinetics of these rearrangements were followed by NMR spectroscopy, giving estimated free energy barriers ($\Delta G^{\#}$) of 25-30 kcal/mol.[42] Surprisingly, the $(RuCp)^+$ complex of the unsubstituted corannulene (related to acecorannulene, but somewhat more planar) shows no variable-temperature ^1H *dynamic NMR effects* up to 140°C (in $C_2D_2Cl_4$). This rules out the intramolecular movement of the arenophile $(RuCp)^+$ OMG around the corannulene surface.[42] In fact, all attempts to detect IRHRs in the $(RuCp)^+$ complexes of planar PAHs such as *pyrene*, *acenaphthylene* and *fluoranthene* in polar solvents were unsuccessful, which was proved by the lack of NMR signal broadening in CH_3NO_2 even at the complex decomposition temperature (90°C). These results were supported by DFT calculations.[43]

However, it has been shown by DFT calculations additionally to experimental data that nonpolar solvents can facilitate IRHRs of $[(PAH)MCp]^+$ complexes, because they favor the formation of contact ion pairs (CIPs) with the counter-anion. In such CIPs, anions tend to stabilize the IRHR unsaturated intermediates and transition states. On the other hand, in polar solvents where separated ion pairs (SIPs) are formed, such stabilization cannot occur.[16,17] Indeed, the $\eta^6 \rightleftharpoons \eta^6$-IRHR is sufficiently rapid (hours) in CH_2Cl_2 solution and extremely slow (weeks) in the much more polar acetone. This is consistent with the well-known fact that reaction rates of many processes involving organometallic salts depend on solvent polarity and the ion pair structure.[44-46] In particular, we have shown by DFT calculations that the interactions between the PF_6^- counterion and the Ru-center of $[(\eta^6\text{-naphthalene})RuCp]^+$ in nonpolar solvents can considerably reduce the IRHR activation barriers, thus making the process possible at reasonable temperatures.[16,17]

In our opinion, there exists *another important approach* to facilitate the $\eta^6 \rightleftharpoons \eta^6$-IRHRs in the Group 8 $(MCp)^+$ complexes, apart for varying the solvent polarity. This approach has first been suggested in our preliminary work on the $(CpRu)^+$ complexes.[15] It consists of increasing the size of

the PAH because in that case the metal-PAH bonding becomes weakened, allowing an easier metal migration along the PAH surface. This was already proven for tricarbonyls of the Group 6 metals (Cr, Mo, W) with the middle-sized kekulene and coronene[47] as well as with large-sized graphene[48,49] and nanotubes[50,51] in comparison with PAH of small size such as naphthalene.[11] Sato et al., who compared $(CpRu)^+$ coronene complexes to smaller PAHs,[52] also noted this trend from their theoretical results. However, no experimental or theoretical studies of the effects of this approach have been performed so far for the OMGs of the Group 8 metals.

Here we report the results of the first comprehensive computational study on the effect of the further increase of the PAH model size on the mobility of the Group 8 $(MCp)^+$ complexes on the PAH surface. The PAH model was increased by adding two additional outer shells of six-member rings around the initial central coronene core. The resulting 4-shell model of graphene (**Gr4**) features a $C_{96}H_{24}$ PAH of D_{6h} symmetry (Fig. 1). The two most inner rings of the large **Gr4** were chosen to be complexed by $(CpM)^+$ in order to mimic realistic graphene species. Although the ML_n OMGs prefer to coordinate with peripheral rings of PAH,[38,39,50-52] this choice was driven by the statistical significance of the central location in pristine graphene.[15] Moreover, it has been previously shown that IRHR activation barriers depend poorly on the OMG localization on the sheet of large PAH ligands,[48,49] which further justifies our choice of the ML_n OMGs localization. The investigated $[(\eta^6\text{-}C_{96}H_{24})MCp]^+$ (M = Fe, Ru, Os) complexes (**1** and **2**) are shown in Fig. 1. To study the ground states, reaction intermediates and transition states of the $\eta^6 \rightleftharpoons \eta^6$-IRHRs of these complexes, the density functional theory using scalar-relativistic approach was employed.

Furthermore, it is important to note that large PAHs such as graphene and nanotubes were shown to have intrinsic anticancer activity,[53,54] and many arene complexes of Ru and Os have been proven to possess anticancer activity as well.[33,36,55,56] Therefore, we suppose that coordinating Ru or Os to very large PAHs could synergistically increase the anticancer activity, thus reinforcing the interest for the stability, bonding and dynamical properties of the complexes **1** and **2**. To the best of our knowledge, it is the first computational study that addresses the structural and dynamic behavior of the metalcyclopentadienyl complexes $(MCp)^+$ (M = Fe, Ru, Os) of a large polyaromatic hydrogenated hydrocarbon (PAH) ($C_{96}H_{24}$) as a model for pristine graphene. The energy barriers of the $\eta^6 \rightleftharpoons \eta^6$ interring haptotropic rearrangement (IRHR) of the $(MCp)^+$ unit between six-membered rings **1** $\rightleftharpoons$ **2** were found to be 30, 27, and 29 kcal/mol for M = Fe, Ru, and Os, respectively. These values are significantly lower than the values found previously theoretically and experimentally for smaller PAHs. Solvent effects in two solvents, nonpolar cyclohexane and polar

acetonitrile, were evaluated as well and were shown not to have significant effects on these energy barriers.

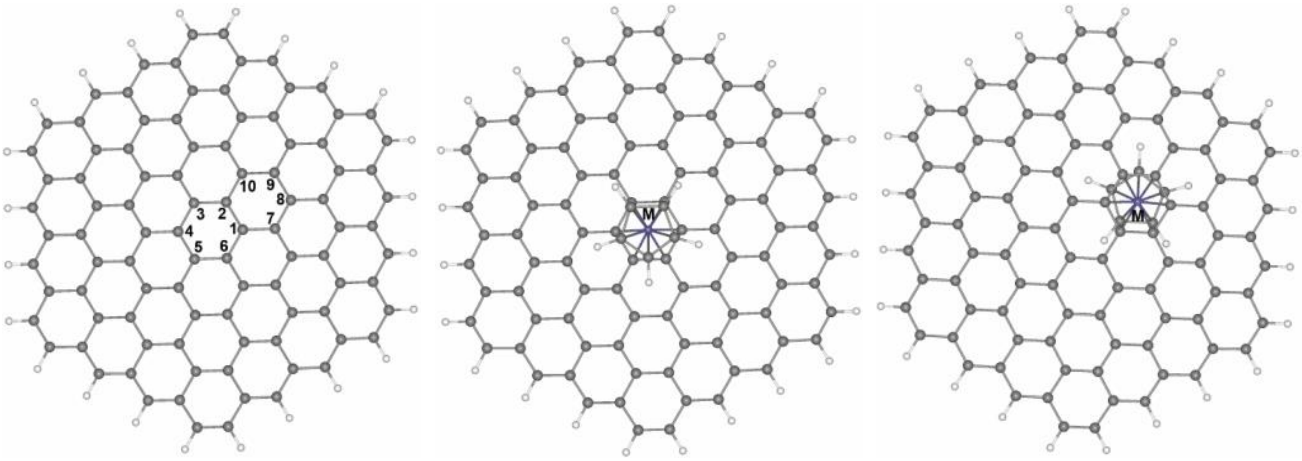

Gr4 [(c-**Gr4**)MCp]$^+$ (**1**) [(n-**Gr4**)MCp]$^+$ (**2**)

Fig. 1. The ligand **Gr4** ($C_{96}H_{24}$) and its $(CpM)^+$ complexes **1** (c - central position) and **2** (n - near central position) considered in this work.

RESULTS AND DISCUSSION

General Features of the Complexes 1 and 2. The DFT-optimized structures of **1** and **2** are basically the same for the three metals (Fig. 1). Zooms on the local metal coordination sphere are shown in Fig. 2, with numbering of the key atoms. Relevant computed bond distances and bond orders are provided in Tables 1 and 2. As can be seen, in the complexes **1** all the 6 M-C bond distances are for each of three metals considered essentially the same, and the complexes **2** the 6 M-C bond distances are divided into two distinctive groups for each of three metals, with bond distance differences within 0.006—0.009 Å. These results are consistent with the expected regular η^6-structures of **1** and **2**. Their calculated geometries agree well with the X-ray structures of [(η^6-naphthalene)MCp]$^{+}$[14] and with the DFT results for other $(MCp)^+$ PAH complexes.[15-17] As expected, both complexes are very close in energy, their free energy difference lying in the range of ~2 kcal/mol (see below). The Mulliken bond orders in complexes **1** and **2** are the same for each metal, and have relatively low values, 0.10—0.14. Their values decrease from Fe to Ru and then increase again to Os, whose complexes have the highest Mulliken bond orders.

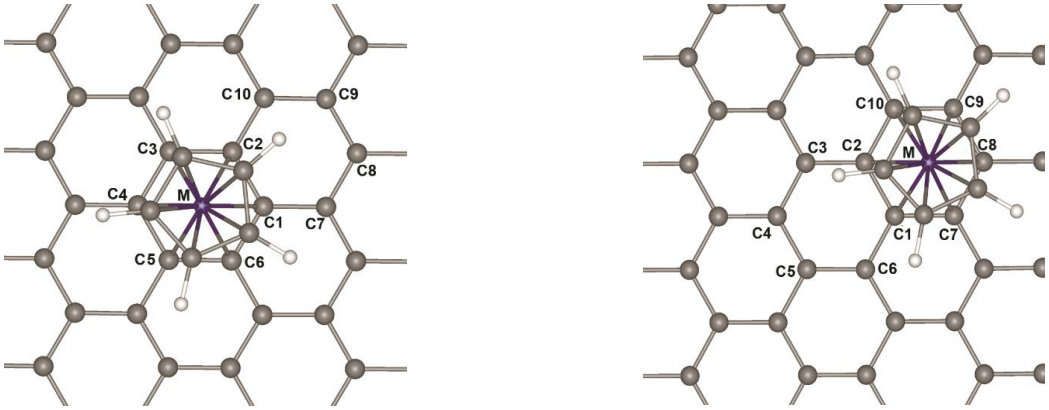

1 **2**

Fig. 2. Metal coordination sphere in complexes **1** and **2** (M = Fe, Ru, Os).

Table 1. Metal-carbon bond lengths (in Å) in **1**, with corresponding Mulliken bond orders in parentheses.

	Fe	Ru	Os
M-C1	2.146 (0.10)	2.296 (0.09)	2.291 (0.13)
M-C2	2.147 (0.11)	2.297 (0.09)	2.291 (0.14)
M-C3	2.147 (0.11)	2.297 (0.09)	2.291 (0.13)
M-C4	2.146 (0.11)	2.297 (0.09)	2.290 (0.13)
M-C5	2.146 (0.10)	2.296 (0.09)	2.290 (0.13)
M-C6	2.146 (0.10)	2.296 (0.09)	2.291 (0.13)

Table 2. Metal-carbon bond lengths (in Å) in **2**, with corresponding Mulliken bond orders in parentheses.

	Fe	Ru	Os
M-C1	2.146 (0.11)	2.294 (0.09)	2.288 (0.14)
M- C2	2.146 (0.11)	2.294 (0.09)	2.289 (0.14)
M- C7	2.144 (0.10)	2.291 (0.09)	2.287 (0.13)
M- C8	2.137 (0.11)	2.285 (0.09)	2.281 (0.14)
M- C9	2.137 (0.11)	2.285 (0.09)	2.281 (0.14)
M- C10	2.143 (0.11)	2.291 (0.09)	2.287 (0.14)

Transition States and Intermediates of the $\eta^6 \rightleftharpoons \eta^6$-IRHR. The $\eta^6 \rightleftharpoons \eta^6$-IRHR corresponding to the **1** $\rightleftharpoons$ **2** interconversion through the OMG shift between two neighboring carbon rings was found to occur for all three metals via an intermediate **IM** flanked by two transition states **TS1** and **TS2** (Scheme 3). The imaginary frequencies of the **TS1** and **TS2** steadily become more negative from Fe and further to Os. Interestingly, for both Fe and Os the imaginary frequency value becomes more negative from the **TS1** to **TS2**, whereas for Ru both TSs have the same imaginary frequency values (Table 3). The coordination mode of these three stationary points (Fig. 3) is best described as η^4, as can be seen from the M-C distances and bond orders given in

Table 3. For all three metals, the intermediate **IM** and two transition states **TS1** and **TS2** have quite similar structures and are very close in energy (Table 4). Generally, the Mulliken bond orders in the **IM**, **TS1** and **TS2**, as expected, are lower than in **1** and **2** (cf. Tables 1-3). Also, these bond orders for Ru are slightly lower in general than for Fe, and for Os they are higher compared to two other metals. In these three closely related structures, the MCp group lies on top of C1, a carbon atom common to the two C_6 rings involved in the IRHR. Thus, the metal in stationary points **TS1**, **IM** and **TS2** is in closest bonding contact with C1 as well as with the three other carbon atoms, namely C2, C6 and C7, participating in the rearrangement.

$$\eta^6\text{-}\mathbf{1} \rightleftharpoons \eta^4\text{-}\mathbf{TS1} \rightleftharpoons \eta^4\text{-}\mathbf{IM} \rightleftharpoons \eta^4\text{-}\mathbf{TS2} \rightleftharpoons \eta^6\text{-}\mathbf{2}$$

Scheme 3. Mechanism of η^6-**1** $\rightleftharpoons$ η^6-**2** IRHR (M = Fe, Ru, Os).

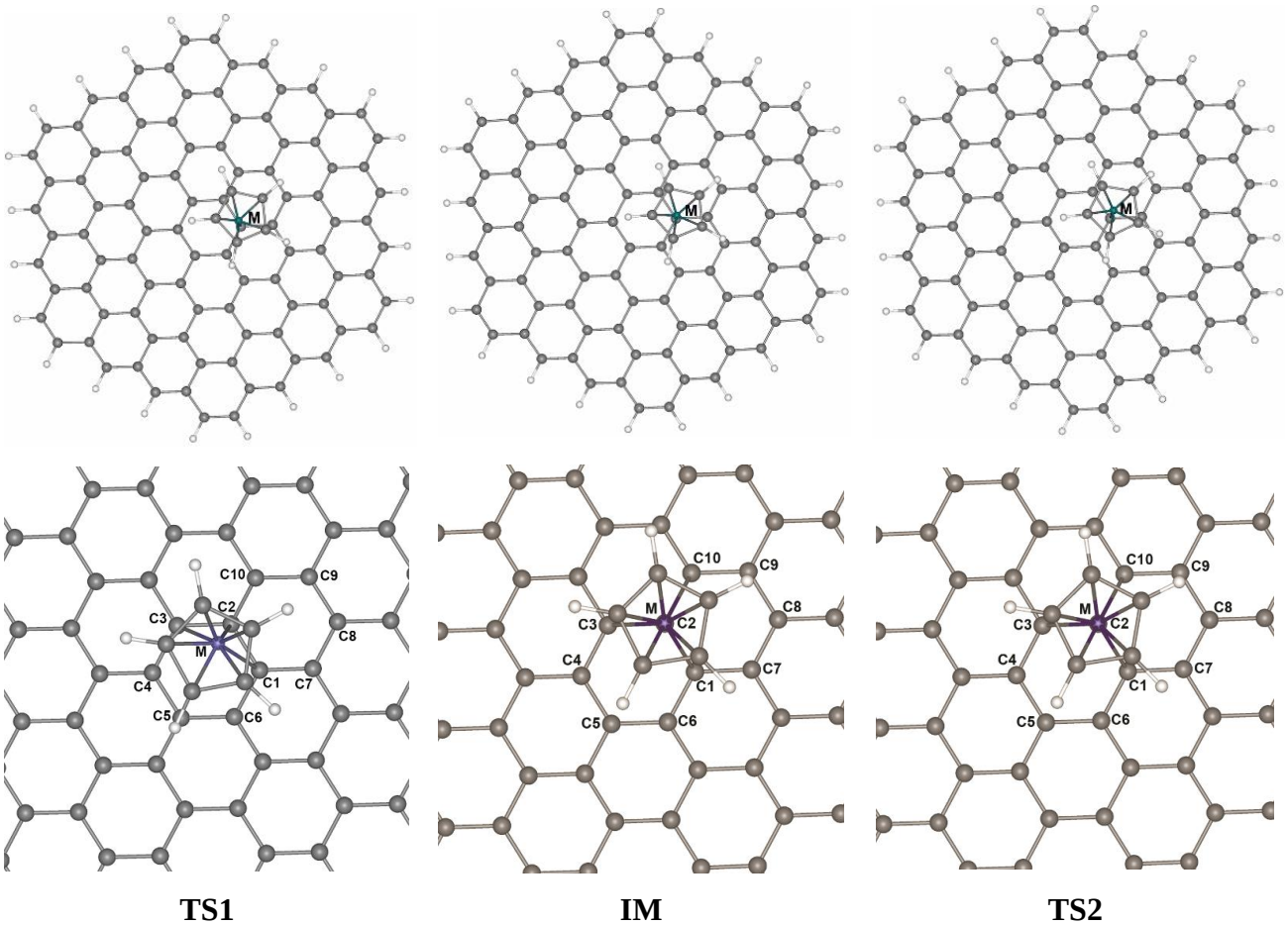

TS1 **IM** **TS2**

Fig 3. General (top) and MCp-zoomed (bottom) views of the **TS1**, **IM** and **TS2** stationary points along the η^6-**1** $\rightleftharpoons$ η^6-**2** IRHR (M = Fe, Ru, Os).

Table 3. Metal-carbon-bond lengths (in Å) in **TS1**, **IM**, and **TS2**, with corresponding Mulliken bond orders in parentheses. The unique imaginary vibrational frequency found for every transition state is given in cm^{-1}.

Metal	Fe			Ru			Os		
bond lengths	TS1 (ω_{im} = 14i)	IM	TS2 (ω_{im} = 34i)	TS1 (ω_{im} = 95i)	IM	TS2 (ω_{im} = 95i)	TS1 (ω_{im} = 93i)	IM	TS2 (ω_{im} = 100i)
M-C1	1.980 (0.10)	1.942 (0.08)	1.987 (0.10)	2.139 (0.08)	2.113 (0.07)	2.150 (0.11)	2.121 (0.13)	2.064 (0.13)	2.124 (0.14)
M-C2	2.289 (0.12)	2.314 (0.11)	2.283 (0.12)	2.479 (0.10)	2.494 (0.11)	2.473 (0.11)	2.414 (0.15)	2.447 (0.15)	2.411 (0.15)
M-C6	2.290 (0.12)	2.323 (0.11)	2.549 (0.08)	2.479 (0.10)	2.496 (0.11)	2.651 (0.11)	2.414 (0.15)	2.450 (0.15)	2.710 (0.09)
M-C7	2.530 (0.08)	2.346 (0.11)	2.296 (0.12)	2.623 (0.10)	2.517 (0.11)	2.487 (0.11)	2.701 (0.10)	2.462 (0.16)	2.421 (0.16)

Table 4. Relative total (ΔE) and free (ΔG) energies, kcal/mol, of all the stationary points on the η^6-**1** ⟛ η^6-**2** reaction pathway.

	Fe		Ru		Os	
	L1	L2	L1	L2	L1	L2
1	0	0	0	0	0	0
IM	30.8 (28.8)	31.1 (29.2)	28.3 (25.0)	28.4 (26.5)	28.7 (26.6)	29.0 (27.8)
TS1	31.3 (29.9)	31.5 (30.0)	28.2 (25.5)	28.6 (27.1)	29.9 (29.1)	30.3 (29.5)
TS2	31.7 (30.2)	31.9 (30.4)	28.7 (23.0)	29.0 (28.4)	30.3 (29.4)	30.7 (29.2)
2	-2.2 (-2.5)	-2.1 (-2.3)	-1.6 (-2.5)	-1.8 (-1.8)	-2.0 (-1.4)	-1.9 (0.0)

Noteworthy, the computed IRHR activation barriers $\Delta G^{\#} \approx$ 28-30 kcal/mol (see Table 4) are significantly lower than the activation barriers computed for the similar processes in $(MCp)^+$ (M = Fe, Ru, Os) complexes of the middle size PAHs ($\Delta G^{\#} \approx$ 36-41 kcal/mol).[14,41] In the Group 8 triad, the largest activation barrier is found for Fe and the lowest for Ru, the Os case being intermediate. This is in line with what we found earlier for the similar systems of the Group 6 metals (Cr, Mo, W): the second metal of the triad affords the smallest IRHR activation barrier.[48,49]

Table 5. Morokuma-Ziegler EDA results for the species **1**, **TS1**, **IM**, **TS2** and **2** for M = Fe, Ru and Os.[a] Values are given in eV.

M	Fe					Ru					Os				
	1	TS1	IM	TS2	2	1	TS1	IM	TS2	2	1	TS1	IM	TS2	2
E_{Pauli}[b]	5.89	4.52	5.04	4.44	5.97	7.17	5.15	5.54	4.98	7.33	9.02	6.74	7.84	6.67	9.18
E_{elstat}[c]	-3.59	-3.04	-3.35	-3.00	-3.64	-4.39	-3.45	-3.67	-3.34	-4.49	-5.55	-4.49	-5.21	-4.45	-5.65
E_{orb}[d]	-6.71	-4.50	-4.78	-4.45	-6.83	-6.63	-4.23	-4.43	-4.13	-6.80	-8.15	-5.51	-6.03	-5.45	-8.31
TBE[e]	-4.41	-3.02	-3.09	-3.00	-4.50	-3.85	-2.53	-2.56	-2.49	-3.95	-4.68	-3.26	-3.40	-3.24	-4.77

[a]The considered fragments are **Gr4** and $(MCp)^+$;

[b]E_{Pauli}= Pauli repulsion energy;

[c]E_{elstat} = electrostatic interaction energy;

[d]E_{orb} = orbital interaction energy;

[e]TBE = (total bonding energy) = $E_{Pauli} + E_{elstat} + E_{orb}$.

Energy Decomposition Analysis Results. A deeper insight into the bonding variations along the IRHR process is provided by the energy decomposition analysis (EDA) carried out with the ADF program (see Methods). In this analysis various contributions in the interactions between the **Gr4** ligand and the $(MCp)^+$ (M = Fe, Ru, Os) OMG are considered. The EDA components of the five stationary points for the three considered metals are provided in Table 5. Unsurprisingly, the total bonding energies (TBE) variation along the IRHR pathways follow the corresponding ΔE and ΔG variations shown in Table 4, with nearly degenerate **TS1** and **TS2** transition states.

It can be seen that the TBE absolute values computed for M = Ru are the lowest of the triad. These results are explained by the combination of the lower values of the absolute value of the E_{orb} component (smaller than for Fe and noticeably smaller than for Os), noticeable values of the Pauli repulsion E_{Pauli} component (higher than for Fe but smaller than for Os), and the electrostatic repulsion energy E_{elstat} values which are again intermediate between the values for Fe and Os. This indicates weaker covalent interactions for Ru. Thus, unsurprisingly, the less strongly bonded metal shows the lowest overall energy variation during the IRHR process, and consequently the lowest activation energy.

On the other hand, the largest TBE absolute value is computed for Os, with which not the largest but the intermediate energy barrier is associated. In fact, the Fe/Os ordering depends also on the relative variation of all the EDA components. In the case of Os, the largest variation (weakening) of the E_{Pauli} and E_{elstat} components can be noted when going from **1** to **TS1** or **TS2**, which is clearly the result of a metal size effect. Therefore, the fact that the lowest energy barrier is found for M = Ru can be explained by the compensation of several effects.

In the $(MCp)^+$ (M = Fe, Ru, Os) complexes at the **Gr4** model, starting from the configuration **1**, the OMG can continue, of course, to shift through successive $\eta^6 \rightleftharpoons \eta^6$-IRHRs over the plane of **Gr4** to the periphery of the ligand. Thus, the metal can spread over the whole surface of the graphene model according to statistic and thermodynamic preferences. From the obtained results we can draw the conclusion that for the η^6-graphene complexes of $(CpM)^+$ (M = Fe, Ru, Os), thermally induced $\eta^6 \rightleftharpoons \eta^6$-IRHR at relatively low temperatures (70-90°C) is possible and should proceed experimentally with high rate thus distributing OMG over the surface of graphene.

Solvent Effects on the Barrier Heights. We also evaluated the change of the activation energies in the presence of two different solvents: polar acetonitrile and non-polar cyclohexane (see Methods). It turns out that taking into account the implicit solvent effects modifies the energy barriers only slightly. Thus, in acetonitrile the activation energy was calculated to increase by 1.3, 1.1 and 1.4 kcal/mol for M = Fe, Ru, Os, respectively, and in cyclohexane it was computed to

increase by 1.0, 1.1 and 1.0 kcal/mol for M = Fe, Ru, Os, respectively, in comparison with the gas phase. These small values computed on non-relaxed geometries are even likely to be slightly overestimated. Previously, Sato *et al.* found that, in the case of [(η^6-coronene)(CpRu)]$^+$, the difference between the activation barriers in the gas phase and dichloromethane solution (2.5 kcal/mol) is larger than ours, but still relatively small.[52] This can be explained by a stronger binding of $(CpRu)^+$ to the smaller coronene, as compared to graphene.

CONCLUSIONS

The $\eta^6 \rightleftharpoons \eta^6$-IRHRs of the $(MCp)^+$ (M=Fe, Ru, Os) complexes of the large model graphene molecule **Gr4** ($C_{96}H_{24}$, D_{6h} symmetry) have been first time investigated by means of DFT calculations, both in the gas phase and in two implicit solvents, polar acetone and nonpolar cyclohexane. The metal migration on the graphene ligand was shown to proceed through one intermediate **IM** and two transition states **TS1** and **TS2**, which were calculated to have significantly lower energies compared with the migrations of the $(MCp)^+$ complexes on the smaller PAHs. Thus, increasing the PAH size has been demonstrated to lead to the *noticeable reduction of the activation barriers of the thermally induced $\eta^6 \rightleftharpoons \eta^6$-IRHRs* and therefore to facilitate migration of the $(MCp)^+$ group on the graphene surface. The *activation barrier was calculated to have the smallest height for the second metal of the Group 8 triad, Ru*, as previously was found for the related Group 6 tricarbonyl species. Implicit solvent effects, both from polar and nonpolar solvents, were found to have negligible contributions to the activation barriers. These finding can have considerable significance for design of novel catalytic systems based on the graphene-supported organometallic complexes of the Group 8 metals as well as development of novel compounds with potential anticancer activity.

ACKNOWLEDGMENTS

The authors (YFO, IPG) thank Alexander von Humboldt Stiftung (Bonn, Germany) for providing the workstation and some other software accessories on which DFT calculations were partially performed. Part of this work done by Nechaev M. S. in the frame of TIPS RAS State Plan.

METHODS

Modeling of graphene based on PAH of general formula $C_{6n^2}H_{6n}$, n = 1, 2, 3, 4, 5… etc. with the use of DFT was done. Such model showed that activation barrier values of $\eta^6 \rightleftharpoons \eta^6$-IRHR of $(MCp)^+$ from the central part of PAH to the neighboring ring at n = 4 ($C_{96}H_{24}$) with the high degree

of accuracy could be expressed as $\Delta G^{\#}$ = 30, 27 and 29 kcal/mol, for M = Fe, Ru, Os, respectively, and 32 kcal/mol (for Ru on corenene). We made such a conclusion taking into account the compromise between calculation expenditures and accuracy of dissociation energies and activation barrier determination (see data in Supporting Information for n from 1 to 12). These values are much lower than barriers in naphthalene (46.2, 39.4, 45.9 kcal/mol, for Fe, Ru, Os, respectively)[16,17] and coronene (32 kcal/mol).[53,54] Model PAH $C_{6n^2}H_{6n}$ was chosen based on initial benzene and gradual increase of the size by adding rows of linearly fused-benzene rings along one direction of PAH size. Such model converges to the pristine graphene in the course of the n increase. Criteria of such convergence should be (1) stabilization of dissociation energy from the center of the ligand, (2) decrease of the difference of dissociation energies between complexes at the center and neighbor cycles, and (3) stabilization of the activation barrier between central and neighboring (Supporting Information for n from 1 to 12, Tables S1-S6).

The geometries of ground states, reaction intermediates and transition states were optimized without any constraints in the frame of density functional theory (DFT) with the use of the PRIRODA04 program written by Laikov.[57-59] All stationary points on the potential energy surface (PES) were identified by analyzing the energy Hessians. The Gibbs free energies (G) at 298.15 K were calculated using the approximation of restricted rotator and harmonic oscillator. The generalized gradient approximation PBE functional[60,61] and scalar-relativistic theory were employed, the latter employing the four-component spin-free Hamiltonian derived by Dyall[62] and applied variationally. The all-electron basis sets L1 and L2 were used, where L1 and L2 stand for double and triple set size, respectively. The numbers of contracted and primitive Gaussians used in L1 are respectively {2,1}/{6,2} for H, {3,2,1}/{10,7,3} for C, {6,5,3,1}/{21,16,11,5} for Fe, {7,6,4,1}/{26,23,16,5} for Ru, and {8,7,5,2}/{30,29,20,14} for Os. The numbers of contracted and primitive Gaussians used in L2 are {3,2,1}/{8,4,2} for H, {4,3,2,1}/{12,8,4,2} for C, {8,7,5,3,1}/{25,20,14,8,4} for Fe, {9,8,6,3,1}/{29,26,18,9,5} for Ru, and {10,9,7,4,1}/{33,32,22,17,4} for Os.[57-59] Since the L1 and L2 basis sets provided very similar results, only the data obtained with the larger L2 set are discussed in the paper. Results obtained with the L1 set are provided in the SI (Tables S1-S5). All reaction paths were found by the intrinsic reaction coordinate (IRC) method.[63] The calculations were performed using the MBC100k cluster at the Joint Supercomputer Center (JSCC) (Moscow, Russia). The interactions between the $(MCp)^+$ and **Gr4** fragments were investigated also within the Morokuma-Ziegler energy decomposition analysis (EDA) framework[64-66] by single-point calculations with the ADF program[67-68] at the ZORA scalar-relativistic level of approximation[69] on the PRIRODA04-optimized structures, employing the PBE functional[60-61] and

the standard TZ2P basis set.[66] Within the EDA analysis, the total bonding energy (TBE) between two fragments is expressed as the sum of three components, the Pauli (or exchange) repulsion (E_{Pauli}), the electrostatic interaction energy (E_{Elstat}), and the orbital interaction energy (E_{orb}). Solvent effects (cyclohexane and acetonitrile) were evaluated through single-point calculations with the ADF program by using the conductor-like screening model (COSMO) of solvation.[70-71]

REFERENCES

1. Davies, S. G. Organotransition Metal Chemistry: Applications to Organic Synthesis. Tetrahedron Organic Chemistry, **2013**, vol. 2, Elsevier, Amsterdam, Netherlands.

2. Alberico, D.; Scott, M. E.; M. Lautens. Aryl−Aryl Bond Formation by Transition-Metal-Catalyzed Direct Arylation. *Chem. Rev.* **2007,** *107*, 174-238.

3. Bae, D.Y.; Kim, Y.; Cha, J.; Lee, E. Early Transition Metal Complexes with Triphenolamine Ligands: Synthesis and Applications. *Coord. Chem. Rev.* **2020**, *419*, 213402.

4. Lerayer, E.; Radal, L.; Nguyen, T. A.; Dwadnia, N.; Cattey, H.; Amardeil, R.; Pirio, N.; Roger, J.; Hierso, J. C. Highly Functionalized Ferrocenes. *Eur. J. Inorg. Chem.* **2020**, *2020*, 419-445.

5. Reznikov, A. N.; Klimochkin, Y. N. Recent Developments in Highly Stereoselective Michael Addition Reactions Catalyzed by Metal Complexes. *Synthesis-Stuttgart* **2020**, *52*, 781-795.

6. Quintana, C.; Cifuentes, M. P.; Humphrey, M. G. Transition Metal Complex/Gold Nanoparticle Hybrid Materials. *Chem. Soc. Rev.* **2020**, *49*, 2316-2341.

7. Shvydkiy, N. V.; Perekalin, D. S. Reactions of Arene Replacement in Transition Metal Complexes. *Coord. Chem. Rev.* **2020**, *411*, 213238.

8. Yamamoto, A. Organotransition-Metal Chemistry: Past Development and Future Outlook. J. *Organomet. Chem.* **2020**, *600*, 159-167.

9. Oprunenko, Y. F. Inter-Ring Haptotropic Rearrangements in π-Complexes of Transition Metals with Polycyclic Aromatic Ligands. *Russ. Chem. Rev.* **2000**, *69*, 683-704.

10. Gridnev, I. D.; Tok, O. L. In: Fluxional Organometallic and Coordination Compounds. Eds: Gielen, M.; Willem, R.; Wrackmeyer, B. Wiley, New York, 2004, 41-81.

11. Oprunenko, Y. F.; Akhmedov, N. G.; Laikov, D. N.; Malyugina, S. G.; Mstislavsky, V. I.; Roznyatovsky, V. A.; Ustynyuk. N. A. Regioselective Synthesis of π-Complexes of Substituted Polycyclic Aromatic Compounds. Experimental (NMR) and Theoretical (DFT) Studies of η^6,η^6-Haptotropic Rearrangements in Naphthalenechromiumtricarbonyl Complexes. *J. Organomet. Chem.* **1999**, *583*, 136-145.

12. Albright, T. A.; Hofmann, P.; Hoffmann, R.; Lillya, C. P.; Dobosh, P. A. Haptotropic Rearrangements of Polyene-ML_n Complexes. 2. Bicyclic Polyene-MCp, $M(CO)_3$ Systems. *J. Am. Chem. Soc.* **1983**, *105*, 3396-3411.

13. Ustynyuk, N. A.; Novikova, L. N.; Oprunenko, Y. F.; Malyugina, S. G.; Ustynyuk, Y. A. Indenyl- and Fluorenyl-Transition Metal Complexes: XI. Intramolecularity of the Haptotropic $\eta^6 \rightleftharpoons \eta^5$ Rearrangements in Fluorenylchromium Tricarbonyl Anions by Crossover Experiments. *J. Organomet. Chem.* **1984**, *277*, 75-84.

14. Perekalin, D. S.; Kudinov, A. R. Cyclopentadienyl Ruthenium Complexes with Naphthalene and Other Polycyclic Aromatic Ligands. *Coord. Chem. Rev.* **2014**, *276*, 153-173.

15. Gloriozov, I. P.; Nechaev, M. S.; Zaitsev, K. V.; Oprunenko, Y. F.; Gam, F.; Saillard, J. Y. DFT Study of Inter-Ring Haptotropic Rearrangement in $CpRu^+$ Complexes of Polycyclic Aromatic Ligands. *J. Organomet. Chem.* **2019**, *889*, 9-14.

16. Fetisov, E. O.; Gloriozov, I. P.; Oprunenko, Y. F.; Saillard, J. Y.; Kahlal, S. Influence of Ion Pairing in Inter-Ring Haptotropic Rearrangements in Cationic Cyclopentadienyl Complexes of Ruthenium with Naphthalene: a DFT Investigation. *Organometallics*, **2013**, *32*, 3512-3520.

17. Fetisov, E. O. Private communication.

18. Makhoul, R.; Sahnoune, H.; Davin, T.; Kahlal, S.; Dorcet, V.; Roisnel, T.; Lapinte, C. Proton-Controlled Regioselective Synthesis of $[Cp^*(dppe)Fe–C\text{-}C\text{-}1\text{-}(\eta^6\text{-}C_{10}H_7)Ru(\eta^5\text{-}Cp](PF_6)$ and Electron-Driven Haptotropic Rearrangement of the $(\eta^5\text{-}Cp)Ru^+$ Arenophile. *Organometallics* **2014**, *33*, 4792-4802.

19. Oprunenko, Y. F.; Gloriozov, I. P. Intramolecular Inter-Ring Haptotropic Rearrangement in Iridium Naphthalene Complexes: a DFT Study. *Russ. Chem. Bull.* **2010**, *59*, 2061-2067 and references therein.

20. Oprunenko, Y. F.; Gloriozov, I. P. Intra- and Inter-Ring Haptotropic Rearrangements in Naphthalene and Anthracene Nickel Complexes: a DFT Study. *Russ. Chem. Bull.* **2011**, *60*, 213–222 and references therein.

21. Ashraf, S. M.; Kandioller, W.; Mendoza-Ferri, M. G.; Nazarov, A. A.; Hartinger, C. G.; Keppler, B. K. The Hydration of Chloroacetonitriles Catalyzed by Mono-and Dinuclear Ru^{II}-and Os^{II}-Arene Complexes. *Chem. Biodiv.* **2008**, *5*, 2060-2066.

22. Jeans, R. J.; Chan, A. P. Y.; Riley, L. E.; Taylor, J.; Rosair, G. M. ; Welch, A. J.; Sivaev, I. B. Arene-Ruthenium Complexes of 1,1'-Bis(ortho-carborane): Synthesis, Characterization, and Catalysis. *Inorg. Chem.* **2019**, *58*, 11751-11761.

23. Trifonova, E. A.; Perekalin, D. S.; Loskutova, N. L. ; Nelyubina, Y. V.; Kudinov, A. R. Synthesis of Cyclohexadienyl Ruthenium Complexes by Replacement of the Naphthalene Ligand in [(eta(5)-$C_6H_3Me_4$)Ru(eta(6)-$C_{10}H_8$)]. *J. Organomet. Chem.* **2015**, *785*, 106-111.

24. Matsinha, L. C.; Malatji, P.; Hutton, A. T.; Venter, G. A.; Mapolie, S. F.; Smith, G. S. Water-Soluble Half-Sandwich Ru-II-Arene Complexes: Synthesis, Structure, Electrochemistry, DFT Studies, and Aqueous Phase Hydroformylation of 1-Octene. *Eur. J. Inorg. Chem.* **2013**, 4318-4328.

25. Neumeier, M.; Chakraborty, U.; Schaarschmidt, D.; O'shea, V. D. ; Perez-Ruiz, R.; von Wangelin, A J. Combined Photoredox and Iron Catalysis for the Cyclotrimerization of Alkynes. *Angew. Chem. Int. Ed.* **2020**, *59*, 1-7.

26. Gonzalez-Fernandez, R.; Crochet, P.; Cadierno, V. Cymene-Osmium(II) Complexes with Amino-Phosphane Ligands as Precatalysts for Nitrile Hydration Reactions. *ChemistrySelect* **2018**, *3*, 4324-4329.

27. Coverdale, J. P. C.; Sanchez-Cano, C.; Clarkson, G. J.; Soni, R.; Wills, M.; Sadler, P. J. Easy to Synthesize, Robust Organo-osmium Asymmetric Transfer Hydrogenation Catalysts. *Chem.-Eur. J.* **2015**, *21*, 8043-8046.

28. Soriano, M. L.; Jalon, F. A.; Manzano, B. R;; Maestro, M. Synthesis and Characterization of Ru(Arene) Complexes of Bispyrazolylazines: Catalytic Hydrogen Transfer of Ketones. *Inorg. Chim. Acta* **2009**, *362*, 4486-4492.

29. Mendoza-Ferri, M. G.; Hartinger, C. G.; Nazarov, A. A.; Eichinger, R. E.; Jakupec, M. A.; Severin, K.; Keppler, B. K. Influence of the Arene Ligand, the Number and Type of Metal Centers, and the Leaving Group on the In Vitro Antitumor Activity of Polynuclear Organometallic Compounds. *Organometallics* **2009**, *28*, 6260-6265.

30. Peacock, A. F.; Sadler, P. J. Medicinal Organometallic Chemistry: Designing Metal Arene Complexes as Anticancer Agents. *Chem.-Asian J.* **2008**, *3*, 1890-1899.

31. Thangavel, S.; Paulpandi, M.; Friedrich, H. B.; Murugan, K.; Kalva, S.; Skelton, A. A. Synthesis, Characterization, Antiproliferative and Molecular Docking Study of New Half Sandwich Ir(III), Rh(III) and Ru(II) Complexes. *J. Inorg. Biochem.* **2016**, *159*, 50-61.

32. Sayin, K.; Üngördü, A. Investigation of Anticancer Properties of Caffeinated Complexes via Computational Chemistry Methods. *Spectrochimica Acta Part A: Mol. Biomol. Spectr.* **2018**, *193*, 147-155.

33. Yan Y. K.; Melchart, M.; Habtemariam, A.; Sadler, P. J. Organometallic Chemistry, Biology and Medicine: Ruthenium Arene Anticancer Complexes. *Chem. Commun.* **2005**, 4764-4776.

34. Gupta, G.; Nagesh, N.; Murray, B. S.; Dyson, P. J.; Therrien, B. Antiproliferative Activities of Trithiolato-Bridged Dinuclear Arene Osmium Complexes. *Inorg. Chim. Acta Part A* **2014**, *423*, 31-35.

35. Pettinari, R.; Pettinari, C.; Marchetti, F.; Cavel, C. M.; Scopelliti, R.; Dyson, P. J. Cytotoxicity of Ruthenium-Arene Complexes Containing Beta-Ketoamine Ligands. *Organometallics* **2013**, *32*, 309-316.

36. Zhang, P. Y.; Sadler, P. J. Advances in the Design of Organometallic Anticancer Complexes. *J. Organomet. Chem.* **2017**, *839*, 5-14.

37. Makhoul, R.; Shaw-Taberlet. J. A.; Sahnoune, H.; Dorcet, V.; Kahlal, S.; Halet, J. F.; Lapinte, C. Complexation of the (η^5-Cp)Ru^+ and (η^5-Cp*)Ru^+ Arenophiles on Alkynylnaphthalene: Solvent Effect on the Regioselectivity and the Haptotropic Rearrangement. *Organometallics* **2014**, 33, 6023-6032.

38. Kündig, E. P. Synthesis of Transition Metal η^6-Arene Complexes. In: Transition Metal Arene π-Complexes in Organic Synthesis and Catalysis. Springer, Berlin Heidelberg, 2004, 3-20.

39. Kündig, E. P. Personal communication.

40. Seiders, T. J.; Baldridge, K. K.; O'Connor, J. M.; Siegel, J. S. Ring Selectivity and Migratory Aptitude of Cp*Ru^+ Complexation to Acecorannulene. *Chem. Commun.* **2004**, 950-951.

41. Koefod, R. S.; Mann, K. R. Ring Shift Isomerization Reaction of Monocyclopentadienylruthenium(II) Complexes of Rubrene. Kinetic and Thermodynamic Studies of Metal-Arene Binding Selectivity. *J. Am. Chem. Soc.* **1990**, *112*, 7287-7293.

42. Seiders, T. J.; Baldridge, K. K.; O'Connor, J. M.; Siegel, J. S. Hexahapto Metal Coordination to Curved Polyaromatic Hydrocarbon Surfaces: The First Transition Metal Corannulene Complex. *J. Am. Chem. Soc.* **1997**, *119*, 4781-4782.

43. Rioja, M.; Hamon, P.; Roisnel, T.; Sinbandhit, S.; Fuentealba, M.; Letelier, K.; Saillard J.-Y.; Hamon, J. R. [(η^5-C_5Me_5)Ru]$^+$ Fragments Ligated to Polyaromatic Hydrocarbons: An Experimental and Computational Approach to Pathways for Haptotropic Migration. *Dalton Trans.* **2015**, *44*, 316-329.

44. Macchioni, A. Elucidation of the Solution Structures of Transition Metal Complex Ion Pairs by NOE NMR Experiments. *Eur. J. Inorg. Chem.* **2003**, *2003*, 195-205.

45. Bellachioma, G.; Ciancaleoni, G.; Zuccaccia, C.; Zuccaccia, D.; Macchioni, A. NMR Investigation of Non-Covalent Aggregation of Coordination Compounds Ranging from Dimers and Ion Pairs up to Nano-Aggregates. *Coord. Chem. Rev.* **2008**, *252*, 2224-2238.

46. Lehmann, R. E.; Bockman, T. M.; Kochi, J. K. Concurrent One- and Two-Electron Processes in Electrophile/Nucleophile Interactions of Organometallic Ion Pairs. *J. Am. Chem. Soc.* **1990**, *112*, 458-459.

47. Zhulyaev, N. S.; Gloriozov, I. P.; Oprunenko, Y. F.; Saillard, J.-Y. DFT Study of Chromium Tricarbonyl Complexes of Coronene and Kekulene. *Moscow Univ. Chem. Bull. (Engl. Transl.)* **2017**, *72*, 201-211.

48. Gloriozov, I. P.; Marchal, R.; Saillard, J.-Y.; Oprunenko, Y. F. Chromium Tricarbonyl and Chromium Benzene Complexes of Graphene, Their Properties, Stabilities, and Inter-Ring Haptotropic Rearrangements – A DFT Investigation. *Eur. J. Inorg. Chem.* **2015**, 250-257.

49. Zhulyaev, N. S.; Gloriozov, I. P.; Nechaev, M. S.; Gam, F.; Oprunenko, Y. F.; Saillard, J.-Y. Organometallic Chemistry of New Carbon Materials. Structure and Dynamic Behavior of Group 6 Metal Tricabonyl Complexes of Graphene and Perforated Graphene: a DFT Study. *New J. Chem.* **2019**, *43*, 17991-18002.

50. Nunzi, F.; Mercuri, F.; De Angelis, F.; Sgamellotti, A.; Re, N.; Giannozzi. P. Coordination and Haptotropic Rearrangement of $Cr(CO)_3$ on (n,0) Nanotube Sidewalls: A Dynamical Density Functional Study. *J. Phys. Chem. B* **2004**, *108*, 5243-5249.

51. Zhulyaev, N. S. DFT Study of 6 Group Metal Complexes of Polyaromatic Ligands from Coronene to Graphene. Diploma Thesis (2018) Department of Chemistry, Moscow State University, Moscow, Russia (in Russ.).

52. Sato, H.. Kikumori, C.; Sakaki. S. Solvation Structure of Coronene–Transition Metal Complex: a RISM-SCF Study. *Phys. Chem. Chem. Phys.* **2011**, *13*, 309–313.

53. Iannazzo, D.; Ziccarelli, I.; Pistone, A. Graphene Quantum Dots: Multifunctional Nanoplatforms for Anticancer Therapy. *J. Mat. Chem. B* **2017**, *5*, 6471-6489.

54. Markovic, Z. M.; Harhaji-Trajkovic, L. M.; Todorovic-Markovic, B. M.; Kepić, D. P.; Arsikin, K. M.; Jovanović, S. P.; Trajkovic, V. S. In Vitro Comparison of the Photothermal Anticancer Activity of Graphene Nanoparticles and Carbon Nanotubes. *Biomaterials* **2011**, *32*, 1121-1129.

55. Zeng, L.; Gupta, P.; Chen, Y.; Wang, E.; Ji, L.; Chao, H.; Chen, Z. S. The Development of Anticancer Ruthenium(II) Complexes: from Single Molecule Compounds to Nanomaterials. *Chem. Soc. Rev.* **2017**, *46*, 5771-5804.

56. Moreno, V.; Lorenzo, J.; Aviles, F. X.; Garcia, M. H.; Ribeiro, J. P.; Morais, T. S.; Robalo, M. P. Studies of the Antiproliferative Activity of Ruthenium(II) Cyclopentadienyl-Derived Complexes with Nitrogen Coordinated Ligands. *Bioinorg. Chem. Appl.* **2010**, 1-12.

57. Laikov, D. N. A New Class of Atomic Basis Functions for Accurate Electronic Structure Calculations of Molecules. *Chem. Phys. Lett.* **2005**, *416*, 116-120.

58. Laikov, D. N. Fast Evaluation of Density Functional Exchange-Correlation Terms Using the Expansion of the Electron Density in Auxiliary Basis Sets. *Chem. Phys. Lett.* **1997**, *281*, 151-156.

59. Laikov, D. N.; Ustynyuk, Y. A. PRIRODA-04: a Quantum-Chemical Program Suite. New Possibilities in the Study of Molecular Systems with the Application of Parallel Computing. *Russ. Chem. Bull.* **2005**, *54*. 820-826.

60. Perdew, J. P.; Burke, K.; Ernzerhof, M. Generalized Gradient Approximation Made Simple. *Phys. Rev. Lett.* **1996**, *77*, 3865-3868.

61. Perdew, J. P.; Burke, K.; Ernzerhof, M. Errata: Generalized Gradient Approximation Made Simple. *Phys. Rev. Lett.* **1997**, *78*, 1396.

62. Dyall, K. G. An Exact Separation of the Spin-Free and Spin-Dependent Terms of the Dirac–Coulomb–Breit Hamiltonian. *J. Chem. Phys.* **1994**, *100*, 2118-2127.

63. Gonzalez, C.; Schlegel, H. B. Reaction Path Following in Mass-Weighted Internal Coordinates. *J. Phys. Chem.* **1990**, *94*, 5523-5527.

64. Morokuma, K. Molecular Orbital Studies of Hydrogen Bonds. III. C=O···H–O Hydrogen Bond in $H_2CO\cdots H_2O$ and $H_2CO\cdots 2H_2O$. *J. Chem. Phys.* **1971**, *55*, 1236-1244.

65. T. Ziegler and A. Rauk. A Theoretical Study of the Ethylene-Metal Bond in Complexes between Copper(1+), Silver(1+), Gold(1+), Platinum(0) or Platinum(2+) and Ethylene, Based on the Hartree-Fock-Slater Transition-State Method. *Inorg. Chem.* **1979**, *18*, 1558-1565.

66. te Velde, G.; Bickelhaupt F. M.; van Gisbergen, S. J. A.; Fonseca Guerra, C.; Baerends, E. J.; Snijders, J. G.; Ziegler, T. Chemistry with ADF. *J. Comput. Chem.* **2001**, *22*, 931-967.

67. Fonseca Guerra, C.; Snijders, J. G.; te Velde, G.; Baerends, E. J. Towards an Order-N DFT Method. *Theor. Chem. Acc.* **1998**, *99*, 391-403.

68. Baerends E. J.; Autschbach J.; Bérces A.; Bickelhaupt F. M.; Bo C.; Boerrigter P. M.; Cavallo L.; Chong D. P.; Deng L.; Dickson R. M. et al. ADF2016, SCM, Theoretical Chemistry, Vrije Universiteit, Amsterdam, The Netherlands, http://www.scm.com.

69. Van Lenthe, E.; Baerends, E.-J.; Snijders, J. G. Relativistic Total Energy Using Regular Approximations. *J. Chem. Phys.* **1994**, *101*, 9783-9792.

70. Pye, C. C.; T. Ziegler, T. An implementation of the conductor-like screening model of solvation within the Amsterdam density functional package. *Theor. Chem. Acc.*, **1999**, *101*, 396-408.

71. Klamt, A.; Schüürmann, G. COSMO: a New Approach to Dielectric Screening in Solvents with Explicit Expressions for the Screening Energy and Its Gradient. *J. Chem. Soc., Perkin Trans.* **1993**, *2*, 799–805.